Observation of high-spin bands with large moments of inertia in ^{124}Xe

Somnath Nag, A. K. Singh, G. B. Hagemann, G. Sletten, B. Herskind, T. Døssing, I. Ragnarsson, H. Hübel, A. Bürger, S. Chmel, A. N. Wilson, J. Rogers, M. P. Carpenter, R. V. F. Janssens, T. L. Khoo, F. G. Kondev, T. Lauritsen, S. Zhu, A. Korichi, E. A. Stefanova, P. Fallon, B. M. Nyakó, J. Timár, and K. Juhász

Observation of high-spin bands with large moments of inertia in ^{124}Xe

Somnath Nag[*] and A. K. Singh

Department of Physics, Indian Institute of Technology Kharagpur, IN-721302, India

G. B. Hagemann, G. Sletten, B. Herskind, and T. Døssing

Niels Bohr Institute, Blegdamsvej 17, DK-2100 Copenhagen, Denmark

I. Ragnarsson

Division of Mathematical Physics, LTH, Lund University, P.O. Box 118, SE-221 Lund, Sweden

H. Hübel, A. Bürger, and S. Chmel

Helmholtz-Institut für Strahlen- und Kernphysik, Universität Bonn, Nussallee 14-16, D-53115 Bonn, Germany

A. N. Wilson and J. Rogers

R. S. P. E., ANU, Canberra, ACT 0200 Australia

M. P. Carpenter, R. V. F. Janssens, T. L. Khoo, F. G. Kondev, T. Lauritsen, and S. Zhu

Physics Division, Argonne National Laboratory, Argonne, IL 60439, USA

A. Korichi

CSNSM-IN2P3, F-91405 Orsay Campus, France

E. A. Stefanova

Institute for Nuclear Research and Nuclear Energy, BAS, BG-1784 Sofia, Bulgaria

P. Fallon

Nuclear Science Division, Lawrence Berkeley National Laboratory, Berkeley, California 94720, USA

B. M. Nyakó and J. Timár

Institute for Nuclear Research, Hungarian Academy of Sciences, H-4001 Debrecen, Hungary

K. Juhász[†]

Department of Information Technology, University of Debrecen, H-4010 Debrecen, Hungary

High-spin states in ^{124}Xe have been populated using the ^{80}Se(^{48}Ca, 4n) reaction at a beam energy of 207 MeV and high-multiplicity, γ-ray coincidence events were measured using the Gammasphere spectrometer. Six high-spin bands with large moments of inertia, similar to those observed in neighboring nuclei, have been observed. The experimental results are compared with calculations within the framework of the Cranked Nilsson-Strutinsky model. It is suggested that the configurations of the bands involve excitations of protons across the $Z = 50$ shell gap coupled to neutrons within the $N = 50 - 82$ shell or excited across the $N = 82$ shell closure.

I. INTRODUCTION

[*]Dept. of Physics, NIT Raipur, GE Road, Raipur (C.G.) - 492010
[†]Deceased

Nuclei in the mass - 125 region are known for their softness with respect to γ deformation. Shape changes are induced by a rearrangement of a few valence nucleons. Protons and neutrons occupying $h_{11/2}$ orbitals show op-

posite shape-driving effects as the Fermi surface for protons is located in the lower part of the subshell, whereas it lies in the middle to upper part for the neutrons. As a result, collective and non-collective structures have been found to coexist at low and medium spins [1–6].

Recently, the structure of nuclei in this mass region has been explored up to very high spin where non-collective oblate states were observed as a result of the alignment of all the valence nucleons above the ^{114}Sn core [4–10]. Generation of angular momenta beyond these aligned structures is possible by neutron excitations from this ^{114}Sn core.

Apart from these states, several strongly-deformed high-spin bands extending up to spins $I \sim 50$ - 60 have been observed in ^{120}Te [7] and ^{124}Ba [5] ($N = 68$); ^{122}Te [8] and ^{123}I [11] ($N = 70$); ^{125}Xe ($N = 71$) [12]; ^{125}I [13] and ^{126}Xe [14] ($N = 72$). These bands are weakly populated; in the range of 1-5% of the channel population and, hence, linking transitions were observed only in a few cases [12–14]. From lifetime measurements, deformation parameters $\epsilon_2 \sim 0.25 - 0.35$ were determined for bands in ^{125}Xe [12] and ^{126}Xe [14]. It was suggested that the configuration of the bands involves proton excitations from the $g_{9/2}$ orbital across the Z=50 shell gap and neutron excitations within the 50-82 shells [7, 8, 11, 13]. For the bands in ^{125}I and ^{125}Xe [13, 15], neutron excitations across the N=82 shell gap along with proton excitations from the $g_{9/2}$ orbital across the Z=50 shell gap have been suggested.

The level scheme of ^{124}Xe was investigated in previous studies and collective bands were established up to spin $I \sim 20$ - 30 [3, 16–20]. An extensive level scheme up to $I \sim 35$ with several new rotational bands and non-collective terminating states was reported by Al-Khatib *et al.* [6].

In this article, we present new high-spin results on ^{124}Xe obtained by in-beam γ-ray spectroscopy. Six strongly-deformed high-spin bands were observed to feed the low-lying levels. However, the linking transitions could not be established due to the low population of these sequences. The configurations of the bands are discussed within the framework of the Cranked Nilsson-Strutinsky (CNS) formalism. Tentative spin and parity values have been as-

signed to the bands on the basis of their decay pattern as well as by comparison with the results from the CNS calculations.

II. EXPERIMENTAL DETAILS AND ANALYSIS

Excited states in ^{124}Xe were populated using the ^{80}Se(^{48}Ca,4n)^{124}Xe reaction at a beam energy of 207 MeV. The ^{48}Ca beam, with an intensity of 4 pnA, was provided by the ATLAS accelerator at Argonne National Laboratory. The target consisted of a ^{80}Se layer with a thickness of 600 μg/cm^2 evaporated onto a 300 μg/cm^2 Au backing which faced the beam. The ^{80}Se was protected by 40 μg/cm^2 Au. To avoid heating of the target, it was mounted on four quadrants of a rotating wheel and the incident beam was slightly defocused and wobbled. Gamma-ray coincidence events were measured with the Gammasphere spectrometer [21] consisting of 101 Compton-suppressed Ge detectors at the time of the experiment. A total of 2.7×10^9 events with Ge fold ≥ 4 were recorded in ten days of beam time. In this reaction, the 4n, 5n, p4n, and α4n channels were dominant, populating ^{124}Xe, ^{123}Xe, ^{123}I, and ^{120}Te, respectively. The results on ^{123}I [9, 11] and ^{120}Te [7] have already been published.

Calibrated and gain-matched data were sorted into $\gamma - \gamma$ matrices, $\gamma - \gamma - \gamma$ cubes, and $\gamma - \gamma - \gamma - \gamma$ hypercubes. The software package RADWARE [22] was used in the off-line data analysis.

III. RESULTS AND LEVEL SCHEME

A partial level scheme of ^{124}Xe is displayed in Fig. 1. The low- and medium-spin states have been adopted from the previous work [6]. In the present work, six new rotational bands, $b1 - b6$, feeding low-energy states in the spin 20-25 range, have been observed. With the tentative assignment of spins discussed below, the level scheme is extended to $I \simeq 60$.

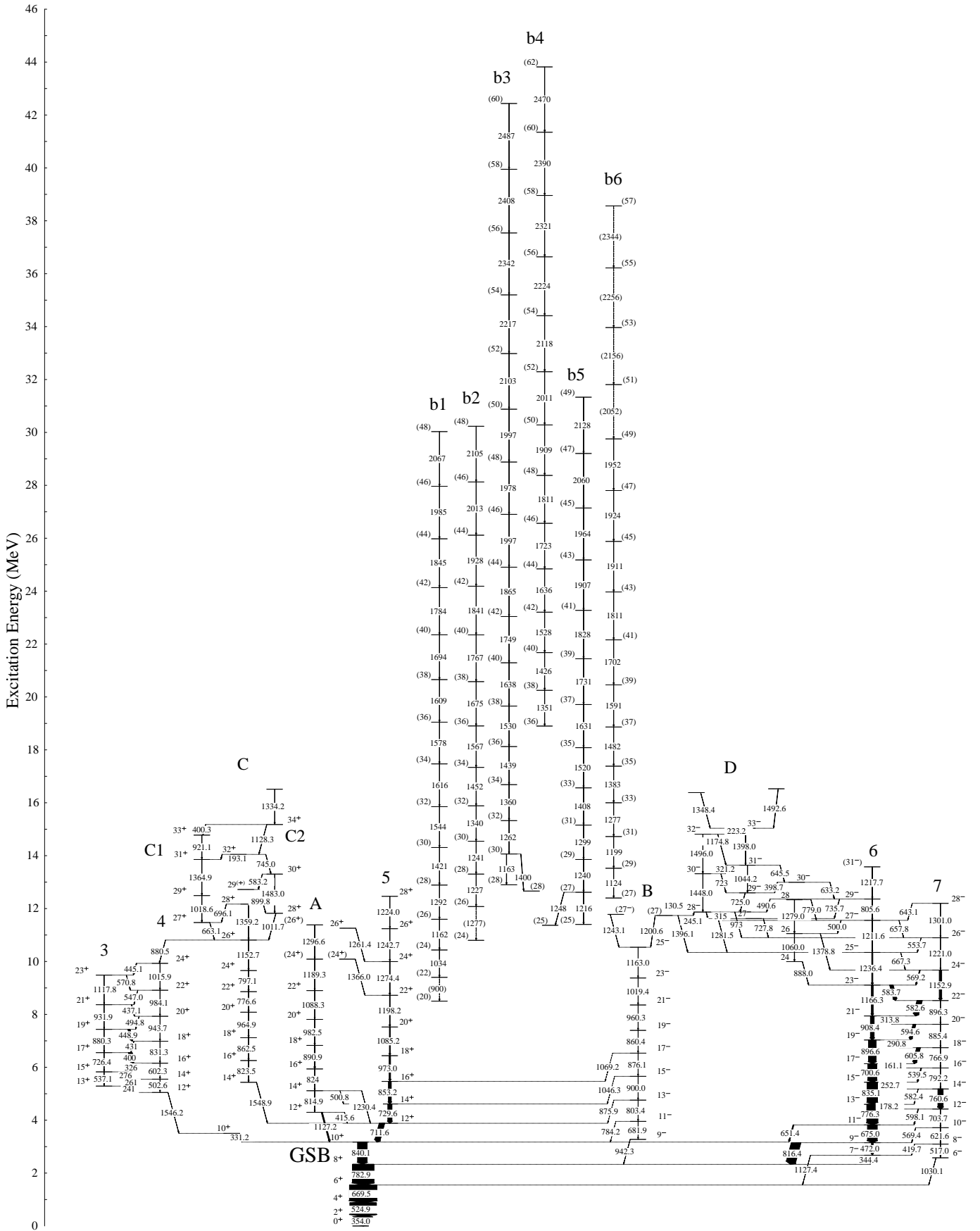Band $b1$ is the most intense one at lower spin with an intensity of $\sim 1.2\%$ with respect to the 782.9-keV tran-

FIG. 1: A partial level scheme of ^{124}Xe. The low- and medium-spin states (structures 1-7 and A-D) have been adopted from Al-Khatib *et al.* [6]. The newly discovered bands are labeled $b1 - b6$.

sition. The sequence becomes unfavored at higher spins, where band $b2$ is most intense with $\sim 1.1\%$, followed by $b3$, $b4$, $b5$, and $b6$ with intensities ranging from ~ 0.8-0.6% with respect to the 782.9-keV transition. These low intensities and the probable fragmentation of the decay-out transitions prevented the observation of firm links between the bands and known lower-spin states. Furthermore, the multipolarity of the in-band transitions could not be determined. An $E2$ multipolarity is adopted as the γ rays involved form regular band structures similar to those observed in neighboring nuclei [12, 14].

The ordering of the transitions within a given band is based on $\gamma - \gamma$ coincidence relationships and on their relative intensities in the $\gamma - \gamma$ coincidence spectra. Summed triple-gated spectra generated with coincidence gates on all the γ rays within each band are displayed in Figs. 2 and 3.
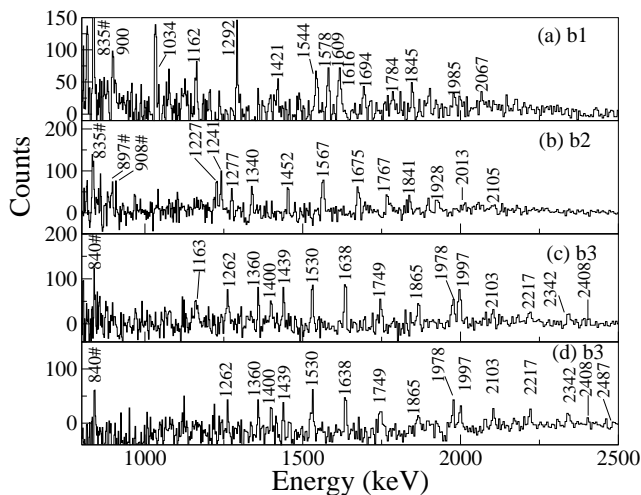

FIG. 2: Summed triple-gated γ-ray coincidence spectra of bands $b1$ - $b3$ in ^{124}Xe. The spectra in panels (a), (b), and (c) were obtained by using triple gates on all transitions of $b1$, $b2$, and $b3$, respectively. The spectrum in panel (d) was produced with a gate on the 1997-keV transition and two gates on all the transitions of $b3$. Transitions marked by # signs in the various panels stem from low-energy levels which receive the highest-intensity feeding from $b1$ - $b3$.

As the bands are not connected to known levels, only estimates of excitation energies and spins are obtained on the basis of the observed decay paths. Based on the relative intensities of the bands, their excitation energies are kept well above the yrast line at angular momenta
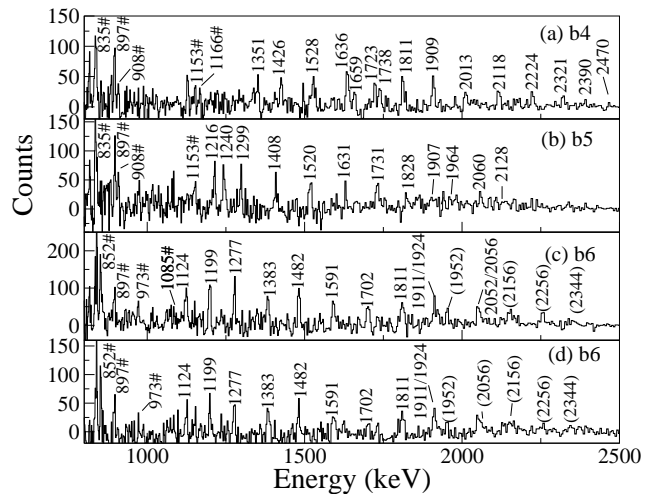

FIG. 3: Summed triple-gated γ-ray coincidence spectra of bands $b4$ - $b6$ in ^{124}Xe. The spectra in panels (a), (b), and (c) were produced by triple gates on all transitions of $b4$, $b5$, and $b6$, respectively. The triple-gated spectrum in panel (d) was obtained with a single gate on the 2052-keV transition and a combination of two gates on all the transitions of band $b6$. Transitions marked by # signs in panels (a) - (d) stem from low-energy levels which receive the highest-intensity feeding from $b4$ - $b6$.

around $26 - 30\hbar$. These were further adjusted within reasonable limits to give agreement with theoretical predictions for the suggested configurations (see below). As a consequence, there may be a variation of 2-3 units in the bandhead spins and, consequently, in the corresponding bandhead energies of $1 - 1.5$ MeV. The adopted values are similar to those of the connected bands in the neighboring nuclei ^{125}Xe [12] and ^{126}Xe [14].

Band $b1$ preferentially feeds the $I^\pi = 17^-$ state of sequence 6 (see Fig. 1). All transitions up to 701 keV are present in the summed triple-gated spectrum produced with transitions of $b1$ (see Fig. 4 (a)). By comparing the experimental data with the results from CNS calculations, an excitation energy of 8.5 MeV has been given to the lowest level of $b1$ with a tentative spin of $I = 20$. This assumes the presence of at least two missing transitions between the lowest level of $b1$ and the 17^- state of sequence 6. With this assignment, band $b1$ extends up to spin $I = 48$. Around $I = 30$, it exhibits an irregularity, indicative of a band crossing.

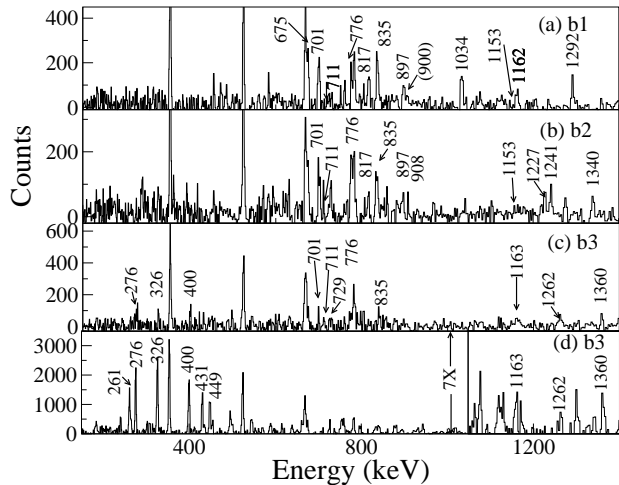Band $b2$ feeds sequences 6 and 7 at levels with spins around $I \sim 21$-22. In the triple-gated spectrum of Fig.

FIG. 4: Summed triple-gated γ-ray spectra showing γ-ray transitions from low-spin states observed in coincidence with transitions of the high-spin bands $b1 - b3$ in ^{124}Xe. For panels (a), (b), and (c), triple gates on all transitions of the respective bands were used. For panel (d), double gates on transitions of band $b3$ and a single gate on each of the transitions with energies 261, 276, 326, 400, 431, 449 keV from sequences 3 and 4 were used. The higher-energy transitions of $b3$ are shown in panel (d) on a magnified scale.

FIG. 5: Summed triple-gated γ-ray spectra showing γ-ray transitions from low-spin states observed in coincidence with transitions of the high-spin bands $b4 - b6$ in ^{124}Xe. For panels (a), (b), and (c), triple gates on all the transitions of the respective bands were used. For panel (d), double gates on transitions of band $b6$ and a single gate on each of the transitions with energies 261, 276, 326, 400, 431, 449 keV from sequences 3 and 4 were used.

4 (b), the 897- and 908-keV transitions are present, but the 1153-keV transition of sequence 7 is missing. A weak 1277-keV transition is observed in coincidence with the $b2$ transitions and is placed tentatively at the bottom of this cascade.

Band $b3$ is the longest sequence among the six new bands observed in this nucleus. It preferentially feeds the levels of sequences 3 and 4 around the 24^+ state. However, a part of the intensity also goes to bands 5 and 6. Figs. 4 (c) and (d) show coincident γ rays of the medium-spin sequences 3 and 4 and the high-spin band $b3$. A branching is observed at the bottom of $b3$, where the 1400-keV γ ray has been placed in parallel with the 1163-keV transition (see Fig.1). Two transitions with energy of 1997 keV were observed in coincidence with the members of $b3$. Indeed, the spectrum in Fig 2 (d) was produced by gating on the 1997-keV γ ray with the rest of the band members. It suggests the presence of a second 1997-keV transition in the band with the placement proposed in Fig. 1. Note that the ordering of the 1997- and 1978-keV transitions is tentative. Comparison with the CNS calculations suggests a tentative spin of $I = 28$ for the
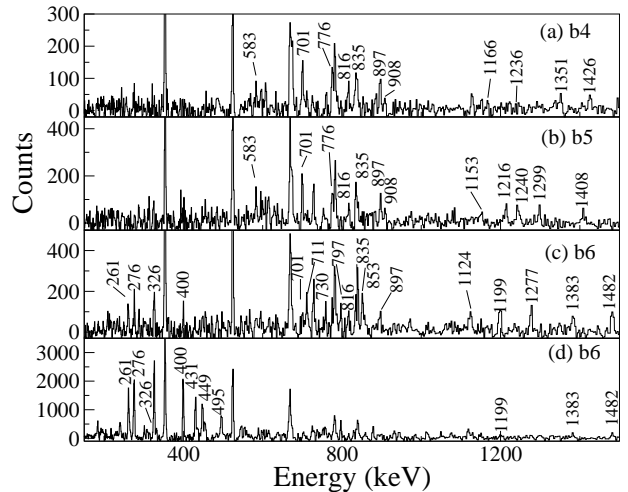
two lowest states. Under this assumption, $b3$ extends up to spin $I = 60$ with a possible band crossing observed around $I \sim 45$.

Band $b4$ has been tentatively assigned with an excitation energy of 18.9 MeV and spin 36 to its lowest state by comparing the properties of the band with the results from the CNS calculations. Thus, this band extends up to $I = 62$. Two transitions with energies of 1659 and 1738 keV were observed in coincidence with the band. However, they could not be placed in the level scheme with certainty, due to their low intensity. The band preferably feeds sequences 6 and 7, where all the transitions below $I^\pi = 25^-$ are observed in the coincidence spectra (see Fig. 5 (a)). Weak decay paths to sequences 3 and 4 are also present.

Band $b5$ primarily decays through sequences 6 and 7 around $I^\pi = 24^-$ (see Fig. 5 (b)). A 1248-keV γ ray has been observed in parallel with the 1216-keV in-band transition. By comparing the band with the results from CNS calculations, a tentative spin of $I = 25$ and an excitation energy of 11.4 MeV have been assigned to the lowest observed level.
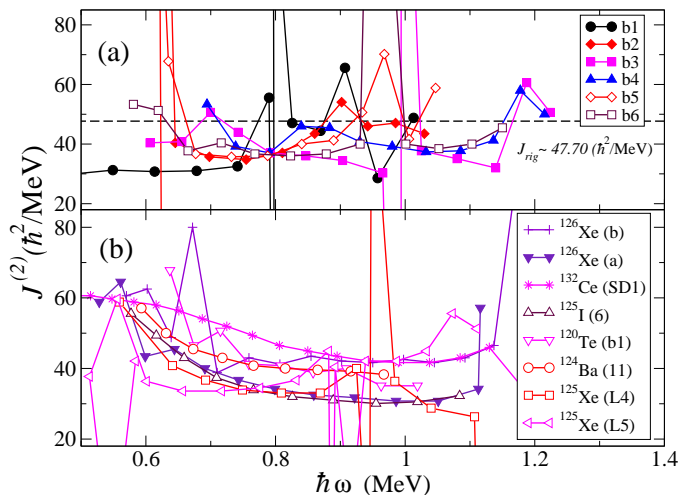
FIG. 6: (Color online) (a) Dynamic moments of inertia, $J^{(2)}$, as a function of rotational frequency for the six new highly-deformed bands in ^{124}Xe. (b) $J^{(2)}$ vs rotational frequency for similar bands in ^{120}Te [7], ^{125}I [13], ^{125}Xe [12], ^{126}Xe [14], ^{124}Ba [5] and ^{132}Ce [23], respectively.

FIG. 7: (Color online) Spins of states as a function of γ-ray energies depopulating these states for (a) ^{124}Xe and (b) ^{125}Xe [12] and ^{126}Xe [14].

Band $b6$ exhibits multiple decay paths, but decays predominantly through branches 3 and 4, as evident from the presence of the intense 276-, 326-, and 400-keV transitions in Fig. 5 (c). A coincidence spectrum between the transitions of band $b6$ and the dipole γ rays of sequences 3 and 4 is displayed in Fig. 5 (d). The band also decays through sequence 6, where transitions up to 897 keV are seen in the coincidence spectrum in Fig. 5 (c). A further decay path through band 5 is evident, where transitions up to 853 keV are observed. Spin I = 27 is assigned to the lowest state of the band. Thus, $b6$ extends up to $I \sim 57$ with a band crossing observed around spin $I = 45$, similar to the one in $b3$. The variation of the intensities of the γ rays along the band is not smooth. The transitions around the band crossing region; e.g., the 1924- and 1952-keV γ rays, are weaker than the transitions at higher spins. The 1800-, 2055-, and 2065-keV γ rays (not drawn in Fig. 1) were observed in the summed triple-gated spectrum produced with the band transitions, however, their exact positions in the band are not clear due to low statistics in individually gated spectra.
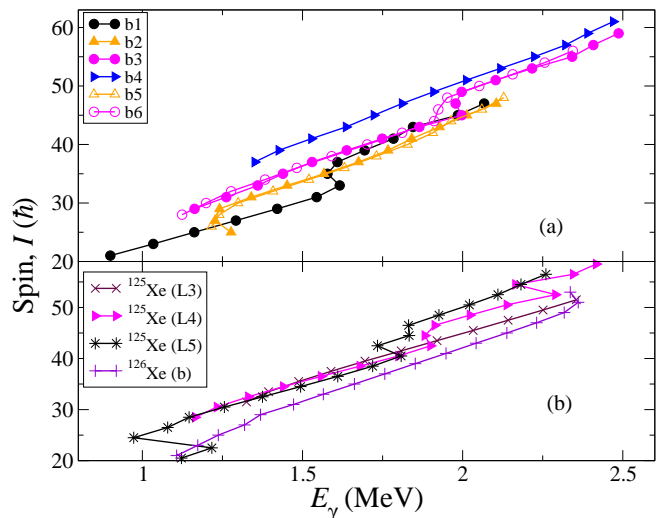
IV. DISCUSSION

The dynamic moments of inertia $J^{(2)}$ are displayed as a function of rotational frequency for the new bands $b1 - b6$ in Fig. 6 (a). While the $J^{(2)}$ values for the bands $b2$, $b4$, and $b5$ are rather smooth, large discontinuities are observed in bands $b1$, $b3$, and $b6$ at $\hbar\omega \sim 0.8 - 1.0$ MeV, indicative of band crossings. For comparison, the moments of inertia of some of the highly-deformed bands of neighboring nuclei can be found in Fig. 6 (b). The moments of inertia for all the bands lie in a narrow range of 40-50 $\hbar^2/MeV$. Band crossings, similar to those of bands $b3$ and $b6$, are also observed in bands $L4$ and $L5$ of ^{125}Xe [12].

The new bands in ^{124}Xe are very similar to the connected bands in ^{125}Xe [12] and ^{126}Xe [14]. Deformation parameters ε_2 between 0.25 and 0.35 were deduced for several of the bands in these latter nuclei [12, 14]. Therefore, similar deformation may be expected for the ^{124}Xe bands. For comparison, the superdeformed band in ^{132}Ce [23], with $\varepsilon_2 \sim 0.4$, is included in Fig. 6(b); its moment of inertia is appreciably larger.

Bands $b1 - b6$ are plotted as a function of transition energy in Fig. 7(a) with the tentative spin values introduced above. An alignment gain of $\simeq 4\hbar$ is observed in $b1$, $b3$, and $b6$. The alignments are compared with those

of the high-spin bands in neighboring ^{125,126}Xe in Fig. 7(b). A similar gain in alignment is observed in bands $L4$ and $L5$ of ^{125}Xe [12].

The CNS formalism [24, 25, 27] has been successfully applied to interpret collective states in several nuclei in this mass region [4, 5, 10, 13]. Within this approach, the orbitals in each $\mathcal{N}$-shell are grouped into high-j and low-j-shells, respectively, where special methods are introduced to make this classification valid in the considered $(\varepsilon_2, \gamma, \varepsilon_4)$ deformation space, see Refs. [28, 29]. Furthermore, each group of high-j or low-j orbitals is divided into two categories with signature $\alpha = 1/2$ and $\alpha = -1/2$. The configurations are then defined by the number of particles in each group. In a shorthand notation, it is only necessary to define the filling of the valence shells, because the low-$\mathcal{N}$ shells are fully occupied while the orbitals in the high-$\mathcal{N}$ shells are empty in the low-energy configurations of ^{124}Xe. These configurations can thus be labeled as $[p_1 p_2, n_1(n_2 n_3)]$. Here, p_1 is the number of proton holes in orbitals of $g_{9/2}$ character, while p_2 is the number of protons in orbitals of $h_{11/2}$ character. Furthermore, the number of neutrons occupying orbitals of $h_{11/2}$, $(h_{9/2}f_{7/2})$, $i_{13/2}$ origin, are represented by n_1, n_2, n_3, respectively. Also, the $\mathcal{N} = 4$ low-j orbitals are partly filled in the low-energy configurations. However, with p_1, p_2, n_1, n_2 and n_3 fixed, the number of particles in these subshells is determined from the condition to get the total number of particles correct, $Z = 54$ and $N = 70$ for ^{124}Xe.

In the present calculations, the κ and μ potential parameters derived for the mass $A \sim 110$ region have been applied [25]. Excitation energies are calculated from the sum of the shell energy and the rotating liquid drop energy. The latter is modelled according to the Lublin-Strasbourg drop (LSD) model [26] with the rigid body moments of inertia calculated with a radius parameter of $r_0 = 1.16$ fm and a diffuseness parameter of $a = 0.6$ fm [27]. An absolute energy scale based on mass excess has been used so that different nuclei can be compared. In the calculations, the energies for different configurations are minimized with respect to the deformation parameters $(\epsilon_2, \epsilon_4, \gamma)$ at various spins. Pairing is not included and, hence, the calculated results are relevant for higher spins, where pairing is quenched. However, the agree-
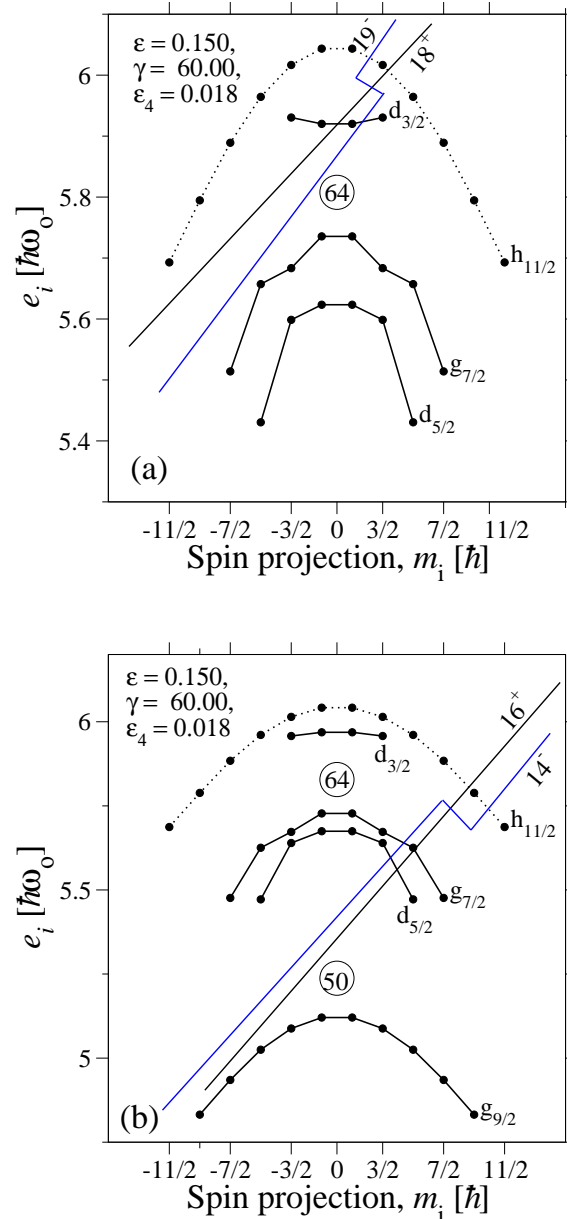

FIG. 8: (Color online) Calculated single-particle energies, e_i, as a function of the spin-projection quantum number, m_i, at $\varepsilon_2 \approx 0.15$, $\gamma = 60°$: (a) for neutrons and (b) for protons. Some low-lying aligned configurations are defined by 'straight-line Fermi surfaces', where the orbitals below the lines are occupied and the total spin is obtained as the sum of the projections m_i below the lines.

ment is also satisfactory at intermediate spins ($I > 15$ in the mass-125 region), see; e.g., Refs. [7, 10, 30].

A. Medium-spin range

The favored aligned neutron configurations, involving particles available outside the ^{114}Sn core, are:

$$\nu[d_{3/2}^2 h_{11/2}^4]; I_{max}^\pi = 18^+;$$
$$\nu[d_{3/2} h_{11/2}^5]; I_{max}^\pi = 19^-.$$

The maximum spin values given here can be inferred from the tilted Fermi surface diagram presented in panel (a) of Fig. 8, where the calculated single-particle energies, e_i, are plotted as a function of the spin-projection quantum number, m_i. The orbitals below the straight lines are occupied and the total spin is obtained as the sum of all projections m_i below the lines.

The favored proton configurations are:

$$\pi[(g_{7/2}, d_{5/2})^2 h_{11/2}^2]; I_{max}^\pi = 16^+;$$
$$\pi[(g_{7/2}, d_{5/2})^3 h_{11/2}]; I_{max}^\pi = 14^-.$$

In this case as well, the maximum spin values are the sum of the projections, m_i, below the straight lines, see panel (b) of Fig. 8. Coupling these configurations to those for the neutrons, provides the I^π quantum numbers for the favored aligned states expected in ^{124}Xe.

The experimental excitation energies, relative to a rotating liquid-drop energy, for the medium-spin states are displayed in Fig. 9(a). For comparison, the new high-spin band $b1$ is included. The calculated energies for some of the low-energy configurations are provided in panel (b) of the figure. Aligned states are highlighted by large open circles and labeled by their spin and parity values.

The non-collective favored states, as observed by Al-Khatib *et al.* [6], are reproduced well by the CNS calculations. The 34^+ level is obtained by coupling the protons in the $[(g_{7/2}, d_{5/2})^2 h_{11/2}^2]$ orbitals with $I_{max}^\pi = 16^+$ to the favored neutron configuration with $I_{max}^\pi = 18^+$. When the neutron configuration with $I^\pi = 19^-$ is coupled to the $[(g_{7/2}, d_{5/2})^3 \, h_{11/2}]_{14^-}$ proton configuration, it may describe the experimentally observed 33^+ state in ^{124}Xe. The maximum spin that can be generated by the full alignment of the angular momenta of all valence nucleons in the configuration $\pi[(g_{7/2}, d_{5/2})^2 h_{11/2}^2] \otimes \nu[d_{3/2}(h_{11/2})^5]$,
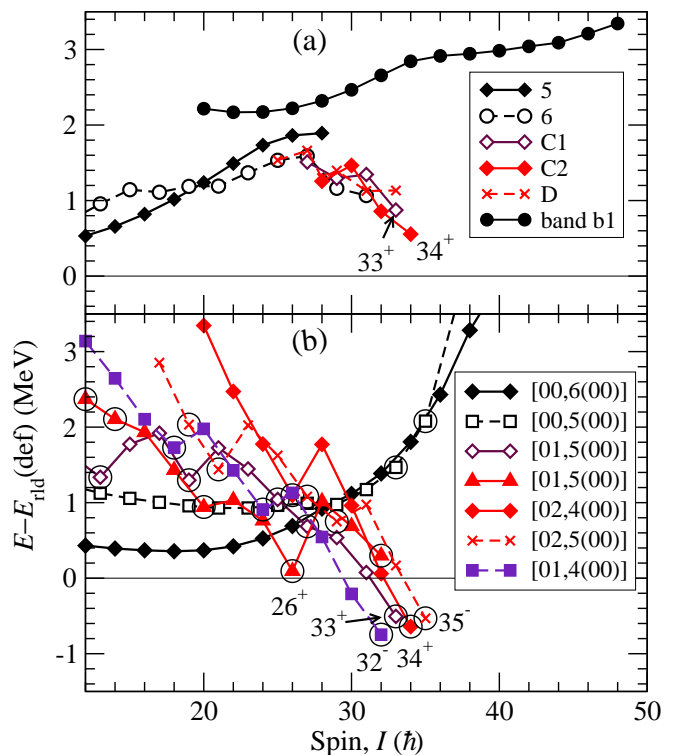

FIG. 9: (Color online) Excitation energies, relative to a rotating liquid drop energy, for observed (a) and calculated (b) valence-space states in ^{124}Xe. Calculated states with spin vectors aligned along the oblate symmetry axis are highlighted by large open circles; states corresponding to experimentally observed levels are labeled by their spins.

or $[02,5(00)]$ in the shorthand notation, is 35^- (see Fig. 9).

B. High-spin states

With the tentative spin assignments to the high-spin bands $b1$ - $b6$ in ^{124}Xe, levels with spin values close to $I \sim 60$ are observed. Excitations within the $Z/N = 50$-82 valence space are not sufficient to describe these levels. One possibility would be to excite neutrons across the $N = 82$ shell gap, but calculations indicate that such configurations alone have a small or low collectivity and cannot explain the observed rotational bands. Structures with higher collectivity are formed if the neutron excitations across the $N=82$ gap are coupled to proton excitations from the $g_{9/2}$ orbitals across the $Z=50$ shell. Configurations involving two-proton excitations $\pi(g_{9/2})^{-2}$ are generally favored in energy, compared to one-proton ones. Total-energy surfaces with the constraint of two $g_{9/2}$ pro-
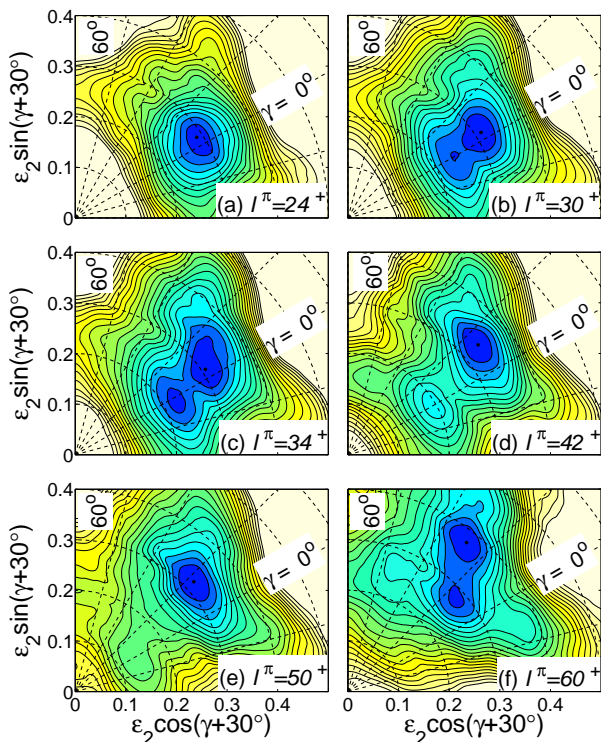
FIG. 10: (Color online) Calculated total-energy surfaces for ^{124}Xe configurations with positive parity and even spins with the extra constraint of the presence of two proton holes in $g_{9/2}$ orbitals. The contour-line separation is 0.25 MeV.

ton holes are presented in Fig. 10, and the lowest calculated bands of this kind, in the $I = 20 - 60$ spin range, are displayed relative to a rotating liquid-drop reference in Fig. 11.

In this figure, configurations with the same number of neutrons excited across the $N = 82$ gap are drawn by the same color. It turns out that among the $\pi(g_{9/2})^{-2}$ configurations, those containing no or three excited particles are, in general, more favored in energy than those with one or two excited particles.

In the $I = 24$ energy surface of Fig. 10 (a), a single prolate minimum appears at $\varepsilon_2 \approx 0.28$, $\gamma \approx 0°$. Fig. 11 indicates that it is formed from configurations with no neutrons excited across the $N = 82$ gap. In general, minima associated with fixed configurations develop towards smaller deformation with increasing spin, while the deformation increases when more particles are excited across closed shells. Thus, at $I = 30$, the '$I = 24$ minimum' has moved to a somewhat smaller deformation, while a new one based on configurations with two particles excited

across the gap is formed at $\varepsilon_2 \approx 0.30$, $\gamma \approx 0°$. These two minima have in turn moved to a smaller deformation at $I = 34$, while the pronounced minimum at $\varepsilon_2 \approx 0.32$ and $\gamma \approx 10°$ seen at $I = 42 - 50$ is associated with the configurations with three neutrons excited across the $N = 82$ gap. Finally, the minimum at $\varepsilon_2 \approx 0.40$ and $\gamma \approx 20°$ in the $I = 60$ surface is associated with configurations involving four excited neutrons (not shown in Fig. 11). The configuration with three excited neutrons is illustrated in Fig. 12, where it corresponds to the filling of the orbitals below the $N = 70$ gap at frequencies, $\hbar\omega \approx 0.6 - 1.2$ MeV. Combined with these neutron configurations, the favored proton one over a large spin range, $I \approx 20 - 60$, corresponds to $\pi(g_{9/2})^{-2}(d_{5/2}g_{7/2})^4(h_{11/2})^2$, see e.g. Fig. 8(a) of Ref. [13].
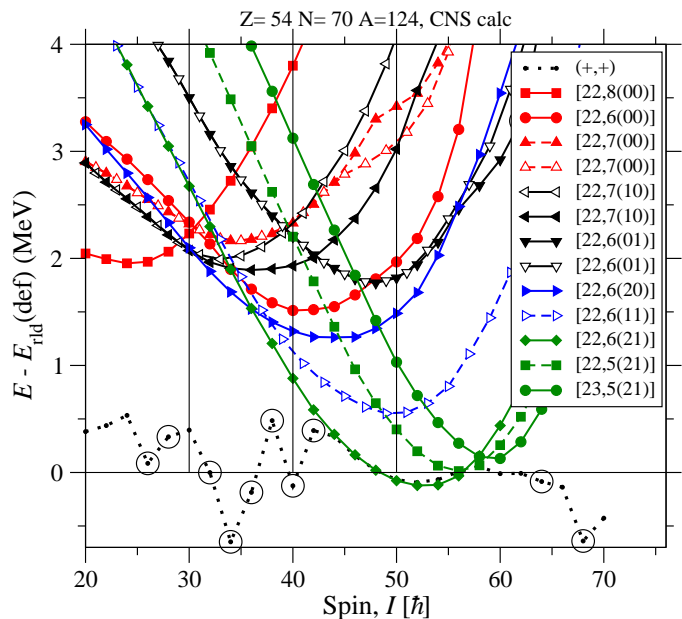

FIG. 11: (Color online) Calculated excitation energies relative to a rotating liquid-drop energy vs spin for some of the lowest energy configurations in ^{124}Xe with two protons excited from the $g_{9/2}$ subshell below the $Z = 50$ gap. Configurations with the same number of neutrons excited across the $N = 82$ gap are drawn with the same color. The positive-parity, even-spin yrast line is shown as a dotted line, indicating that $\pi(g_{9/2})^{-2}$ configurations become yrast just above $I = 40$. Positive (negative) parity configurations are drawn by full (dashed) lines. The even (odd) spin states are shown by closed (open) symbols.

The lowest-energy configurations without particle excitation across the $N = 82$ gap have 6, 7, or 8 $h_{11/2}$ particles; i.e., the [22,6(00)], [22,7(00)], and [22,8(00)] configurations, respectively. It is satisfying that, with the present
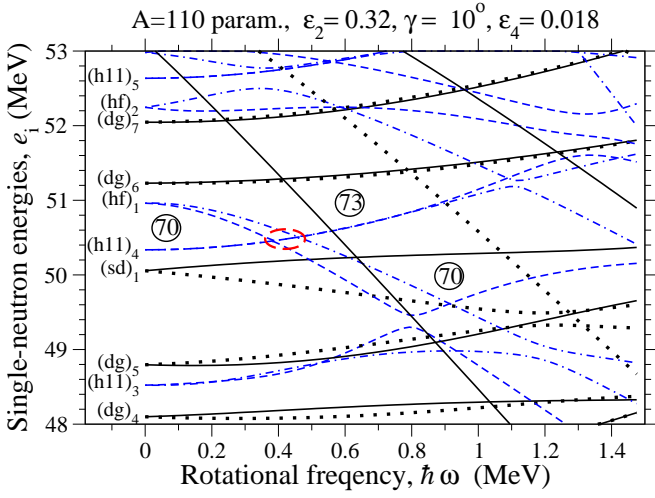
FIG. 12: (Color online) Calculated neutron orbitals as a function of the rotational frequency, $\hbar\omega$, at a deformation typical for the high-spin configurations of ^{124}Xe, $\varepsilon_2 = 0.32$, $\gamma = 10°$, $\varepsilon_4 = 0.018$. The orbitals are labeled at $\hbar\omega = 0$ by their dominant j-shell amplitude and the ordering within the respective groups. The $h_{11/2}$ orbitals are labeled as (h11) while pseudospin partners [32] $d_{5/2}g_{7/2}$, $s_{1/2}d_{3/2}$ and $h_{9/2}f_{7/2}$ as (dg), (sd) and (hf), respectively. Dashed (or dot-dashed) lines are used for negative-parity orbitals while lines with dots are used for signature $\alpha = -1/2$. The crossing between the $(h11)_4$ and $(hf)_1$ orbitals is highlighted with a dashed ellipse.

FIG. 13: (Color online) Comparison between experiment and calculations for bands $b1$, $b2$, $b4$, and $b5$. Observed and corresponding calculated bands are drawn in panels (a) and (b), respectively, with the difference between calculations and experiment being given in panel (c). The convention for lines and symbols is the same as in Fig. 11.

spin values, band $b1$ agrees well with the [22,6(00)] configuration above the crossing and with the [22,8(00)] one below. With pairing included, such configuration changes are expected to result in a smooth band crossing [31], as observed in band $b1$. The agreement between experiment and calculations is illustrated in Fig. 13. Furthermore, bands $b2$ and $b5$ appear to be signature partners and can be assigned to the [22,7(00)] configurations with different signature for the $\mathcal{N} = 4$ neutrons, see Fig. 13. The discontinuities in the calculated [22,7(00)] bands at $I \approx 50$ are caused by a minor shape change from $0°$ to negative γ values which occurs at slightly different spin values for the two signatures.

The most favored configuration with three neutrons excited across the $N = 82$ gap is [22,6(21)]. Because it is calculated to lie lowest over a large spin range, one would expect that it has an experimental correspondence with no band crossing. Indeed, as seen in Fig. 13, band $b4$ is smooth over its full spin range and, with the present spin assignments, it agrees well with the [22,6(21)] configuration.
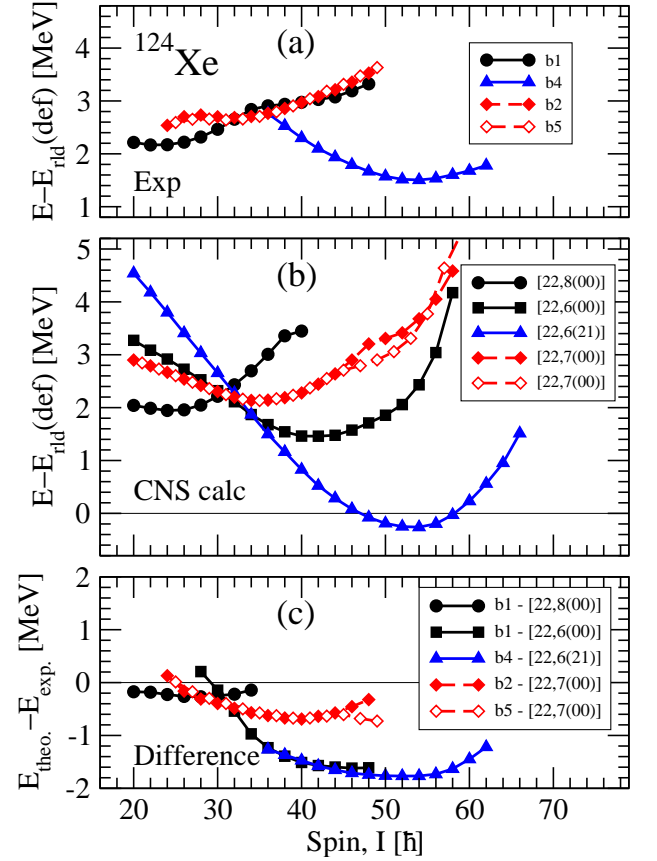
The remaining bands $b3$ and $b6$ appear to be signature partners, going through a band crossing at $I \approx 45$. If tentative transitions are excluded, $b6$ is only observed over a short spin range above the crossing. However, the fact that spins and excitation energies can be chosen such that the bands are close to signature partners through the crossing further supports the existence of the tentative transitions and represents evidence that the relative spins and excitation energies are likely close to the actual values. In the crossing region, 3-4 units of spin are gained. The single-neutron orbitals in Fig. 12 are drawn at a typical deformation for configurations with two or three neutrons excited across the $N = 82$ gap. The interaction between the $(h11)_3$ orbitals and the $(hf)_1$ ones (the labeling of the orbitals is explained and illustrated in Fig. 12) could be responsible for the observed crossing in bands $b3$ and $b6$. However, this interaction does not occur for neutron number $N = 70$, but rather for

$N = 66$. Furthermore, with the large signature splitting in the $(h11)_3$ orbitals, there is no way to explain the observed signature degeneracy below the crossing. Thus, there is no single-particle crossing close to a frequency of 1 MeV which can be responsible for the crossings in bands $b3$ and $b6$. On the other hand, if the crossing between the $(hf)_1$ and the $(h11)_4$ orbitals (marked by a dashed ellipse in Fig. 12) occurred at a higher frequency, it could account for the observation. The crossing can be moved by a parameter change so that the spacing between the $h_{9/2}f_{7/2}$ and the $h_{11/2}$ subshells is increased. One way to achieve such an outcome is to increase the strength of the $l \cdot s$ and l^2 couplings in the $\mathcal{N} = 5$ oscillator shell by the same percentage. It turns out that a rather large increase, by approximately 20%, is required to reproduce the crossing frequency in bands $b3$ and $b6$. The single-neutron orbitals calculated with such an increase are drawn in Fig. 14.
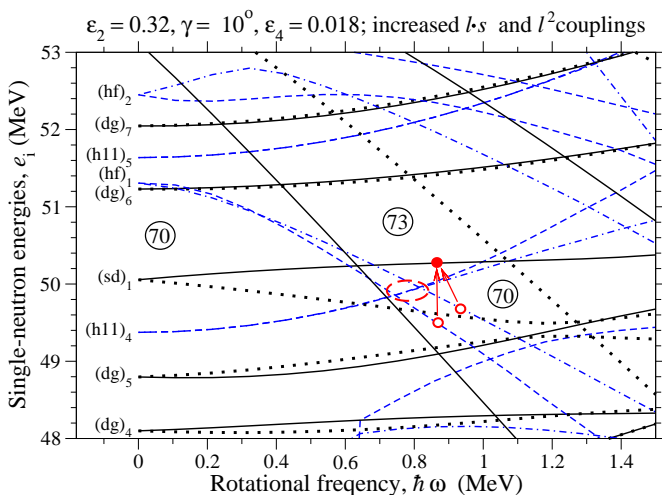

FIG. 14: (Color online) Calculated neutron orbitals at the same deformation as in Fig. 12, but with the $l \cdot s$ and l^2 strengths in the $\mathcal{N} = 5$ oscillator shell increased by approximately 20% relative to the $A = 110$ parameters [25]. Band $b4$ is assigned to the configuration with all orbitals below the $Z = 70$ gap at $\hbar\omega \approx 1.0$ MeV occupied, while one particle is lifted to the $\alpha = 1/2$ $(sd)_1$ orbital according to the arrows in bands $b3$ and $b6$. For lower frequencies in these bands, the odd $(hf)_1$ particle moves to the $(h11)_4$ where these orbitals cross within the ellipse drawn by a dashed line.

The parameter change does not have much influence on band $b4$, which is formed in the $N = 70$ gap marked at $\hbar\omega \approx 1.0$ MeV in Figs. 12 and 14. One possible interpretation is then that the high-spin configurations of bands $b3$ and $b4$ are formed by lifting one neutron

from the two signature branches of the $(hf)_1$ orbital to the $\alpha = 1/2$, $(sd)_1$ orbital as shown by red arrows in Fig. 14. With decreasing frequency, when the $(hf)_1$ orbitals intersect with the $(h11)_4$ orbitals at $\hbar\omega \approx 0.8$ (marked by a dashed ellipsoid in Fig. 14), the odd neutron will jump to the $(h11)_4$ orbitals, i.e. the band crossing observed in bands $b3$ and $b6$ is created. With this interpretation, the band-crossing frequency in bands $b3$ and $b6$ is essentially reproduced in the calculations as illustrated in Fig. 15.

It turns out that bands $b2$ and $b5$ are not much affected by the revised parameters used in Fig. 15, while the band-crossing in $b1$ is moved from $I \approx 31$ using the $A = 110$ parameters (Fig. 13) to $I \approx 38$ with the revised parameters. These values should be compared with the observed crossing at $I \approx 34$, see Fig. 13. The calculated change is caused by a lowering of the Fermi level within the $h_{11/2}$ shell so that the $\nu(h_{11/2})^8$ configuration is favored up to higher spin values, relative to the $\nu(h_{11/2})^6$ configuration. The comparison suggests that a more complete investigation of the single-particle parameters would be desirable. Such an investigation, which should also include the neighboring nuclei, e.g., ^{125,126}Xe, is outside the scope of the present analysis of the high-spin bands in ^{124}Xe.

In Figs. 13 and 15, the differences between calculations and experiment are as expected; they exhibit a small down-slope with increasing spin as anticipated when pairing is not included, see; e.g., Refs. [33, 34]. Furthermore, the signature degeneracy of bands $b3$ and $b6$ is well described at low spin by the fourth $h_{11/2}$ orbital. Contrary to experiment, the calculated bands develop a signature splitting a few spin units before the crossing. This feature could depend on details on how the bands change deformation and this is not considered to be a shortcoming in the present context. Above the crossing, the signature splitting exhibited by bands $b3$ and $b6$ is considerably larger in the calculations than in the data. The calculated splitting depends on the $(hf)_1$ orbital, where signature $\alpha = 1/2$ is favored if the wave function is dominated by the $h_{9/2}$ shell, while $\alpha = -1/2$ is favored in the $f_{7/2}$ shell. Consequently, it should be possible to find relative positions of the $h_{9/2}$ and $f_{7/2}$ shells so that the two signatures of the $(hf)_1$ orbital are close to being signature-degenerate. The energy differences between
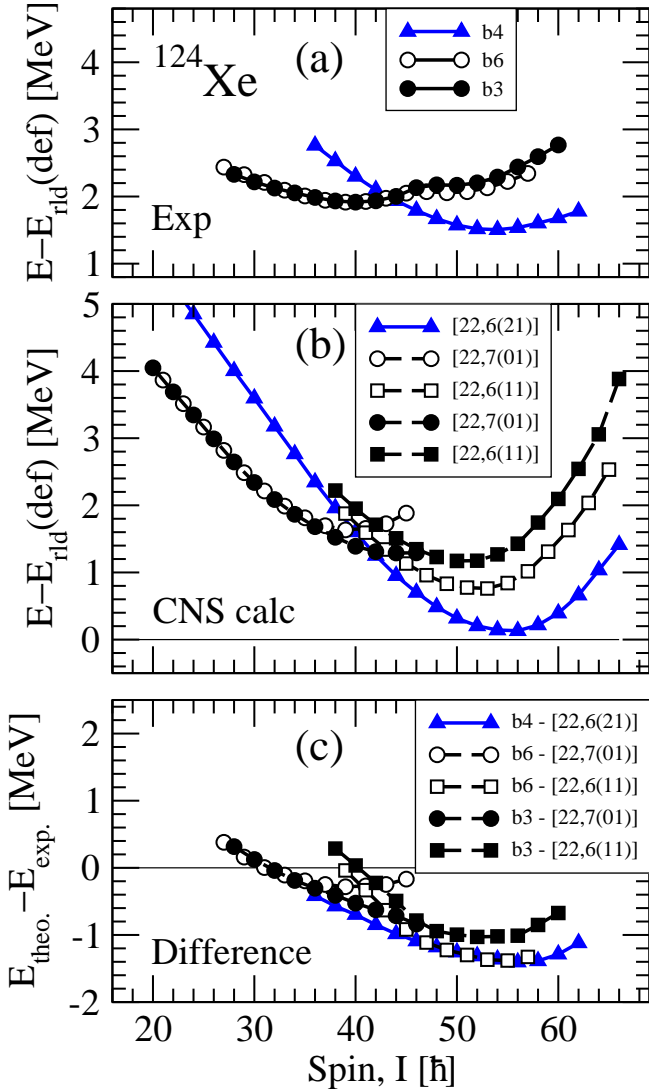
FIG. 15: (Color online) Comparison between (a) experiment and (b) calculations for bands $b4$, $b3$ and $b6$. The calculated results were obtained with the new parameters of Fig. 14. The energy difference between experiment and calculation is shown in (c). The convention for lines and symbols is the same as in Fig. 11.

calculations and experiment tend to increase at very high spins, see Figs. 13 and 15, indicating that the highest-spin states are calculated too high in excitation energy. Similar discrepancies have previously been observed in other nuclei where rotational bands are observed to very high frequencies; e.g., in ^{132}Ce [23] and ^{62}Zn [35]. It is possible that, in a more realistic single-particle potential, the coupling to higher shells will contribute more angular momentum at very high rotational frequencies.

V. CONCLUSIONS

High-spin states in ^{124}Xe were populated in the ^{80}Se(^{48}Ca,4n)^{124}Xe reaction and high-fold γ-ray coincidence events were measured using the Gammasphere spectrometer. Six high-spin bands with large moments of inertia, $b1$-$b6$, were observed to decay into known levels around spin $I \sim 20$. However, no linking transitions were identified between the high-spin sequences and the lower part of the level scheme. Tentative excitation energies and spin assignments to the bands have been proposed on the basis of their decay patterns into the lower-lying levels, their relative intensities, and comparisons with the results of CNS calculations. The calculations indicate that the configurations of the bands involve proton excitations from the $g_{9/2}$ orbitals across the $Z = 50$ shell gap along with neutron excitations within the $N = 50 - 82$ shell or across the $N = 82$ shell gap. The latter excitation leads to more deformed bands involving configurations where $h_{9/2}f_{7/2}$ and $i_{13/2}$ neutron orbitals are occupied. The bands labeled $b3$ and $b6$ are of special interest as they gain 3 - 4 units of angular momentum at a band crossing close to $\hbar\omega = 1$ MeV and appear to be nearly degenerate signature partners. These features cannot be reproduced in the CNS calculations with the standard set of parameters for the mass A=110 region. A possible way to achieve agreement with the experimental results is to increase the spacing between the $h_{11/2}$ and $h_{9/2}f_{7/2}$ subshells in the neutron single-particle potential by a little more than one MeV. However, a broader analysis should be performed in the future to test the effect of such a parameter change on the high-spin collective bands in neighboring nuclei. In this context, it would be very helpful if more collective bands in this region were linked so that their spin values and excitation energies were known.

[1] A. Granderath *et al.*, Nucl. Phys. **A 597**, 427 (1996)
[2] R. Wyss *et al.*, Nucl. Phys. **A 505**, 337 (1989).
[3] V. Werner, H. Meise, I. Wiedenhöver, A. Gade, P. von Brentano, Nucl. Phys. **A 692**, 451 (2001).
[4] A. K. Singh *et al.*, Phys. Rev. C **70**, 034315 (2004).
[5] A.Al-Khatib *et al.*, Phys. Rev. C **74**, 014305 (2006).
[6] A. Al-Khatib *et al.*, Eur. Phys. J. A **36**, 21 (2008).
[7] Somnath Nag *et al.*, Phys. Rev. C **90**, 037302 (2014).
[8] Somnath Nag *et al.*, Phys. Rev. C **88**, 044335 (2013).
[9] Purnima Singh *et al.*, Phys. Rev. C **85**, 034319 (2012).
[10] Purnima Singh *et al.*, Phys. Rev. C **82**, 034301 (2010).
[11] Purnima Singh *et al.*, Phys. Rev. C **86**, 067305 (2012).
[12] A. Al-Khatib *et al.*, Phys. Rev. C **83**, 024306 (2011).
[13] Purnima Singh *et al.*, Phys. Rev. C **84**, 024316 (2011).
[14] C. R. Hansen *et al.*, Phys. Rev. C **76**, 034311 (2007).
[15] I. Ragnarsson, B. G. Carlsson, Hai-Liang, A. Kardan, Purnima Singh, S. Nag, A. K. Singh and H. Hübel, Internat. Nucl. Phys. Conf. INPC 2013, contrib. NS 185.
[16] B. Saha *et al.*, Phys. Rev. C **70**, 034313 (2004).
[17] W. Gast *et al.*, Z. Phys. A **318**, 123 (1984).
[18] I. Schneider *et al.*, Phys. Rev. C **60**, 014312 (1999).
[19] G. Lo Bianco *et al.*, Z. Phys. A **359**, 347 (1997).
[20] G. Rainovski *et al.*, Phys. Rev. C **66**, 014308 (2002).
[21] I. Y. Lee, Nucl. Phys. **A 520**, 641 (1990).
[22] D. C. Radford, Nucl. Instrum. Methods **A 361**, 297 (1995).
[23] E. S. Paul *et al.*, Phys. Rev. C **71**, 054309 (2005).
[24] T. Bengtsson and I. Ragnarsson, Nucl. Phys. **A 436**, 14 (1985).
[25] A. V. Afanasjev, D. B. Fossan, G. J. Lane, and I. Ragnarsson, Phys. Reports **322**, 1 (1999).
[26] K. Pomorski and J. Dudek, Phys. Rev. C **67**, 044316 (2003).
[27] B. G. Carlsson and I. Ragnrasson, Phys. Rev. C **74**, 011302 (2006).
[28] A. V. Afanasjev and I. Ragnarsson, Nucl. Phys. **A 608**, 176 (1996).
[29] I. Ragnarsson *et al.*, Phys. Rev. Lett. **74**, 20 (1995).
[30] K. Starosta *et al.*, Phys. Rev. C **64**, 014304 (2001).
[31] I. Ragnarsson, B.G. Carlsson, A. Kardan and Hai-Liang Ma, Acta Phys. Pol. **B46**, 477 (2015).
[32] A. Bohr, I. Hamamoto, and B. R. Mottelson, Physica Scripta **26**, 267 (1982).
[33] Hai-Liang Ma, B.G. Carlsson, I. Ragnarsson and H. Ryde, Phys. Rev. C **90**, 014316 (2014).
[34] C.M. Petrache *et al.*, Phys. Rev. C **91**, 024302 (2015).
[35] J. Gellanki *et al.*, Phys. Rev. C **86**, 034304 (2012)